Large stiffness thermoformed open cell foams with auxeticity

Qicheng Zhang[1*†], Wenjiang Lu[2†], Fabrizio Scarpa[1], David Barton[3], Roderic S. Lakes[4], Yunpeng Zhu[5], Ziqiang Lang[5], Hua-Xin Peng[2*]

[1.] Bristol Composites Institute (ACCIS), University of Bristol, BS8 1TR Bristol, UK

[2.] Institute for Composites Science Innovation (InCSI), School of Materials Science and Engineering, Zhejiang University, Hangzhou, 310027, PR. China

[3.] Department of Engineering Mathematics, University of Bristol, BS8 1UB Bristol, UK

[4.] Engineering Physics, University of Wisconsin-Madison, 1415 Engineering Drive, Madison, WI 53706

[5.] Department of Automatic Control and Systems Engineering, University of Sheffield, Sheffield, UK

Abstract: Open cell foams with auxeticity and modulus 5 times larger than the stiffest auxetic polymeric open cell foam featured in scientific literature are developed in this paper by using vacuum bags and autoclave following a thermoforming process. The resulting foam is transverse isotropic with microstructures exhibiting elongated semi-reticulated configurations, and contains a plane in which the auxetic behavior is evident. Tensile and compression quasi-static tests were carried out on samples cut along different directions and with different thicknesses. Foams have been also subjected to tensile training at different maximum strains to assess their mechanical performance. The tensile modulus and Poisson' s ratio values of the auxetic foams produced in this work can reach 25MPa and -0.4 in one plane and can feature a negative Poisson' s ratio up to -1.3 for thinner specimens. Smaller thicknesses and higher tensile training strains can also reduce the stiffness but enhance the auxeticity of this porous material.

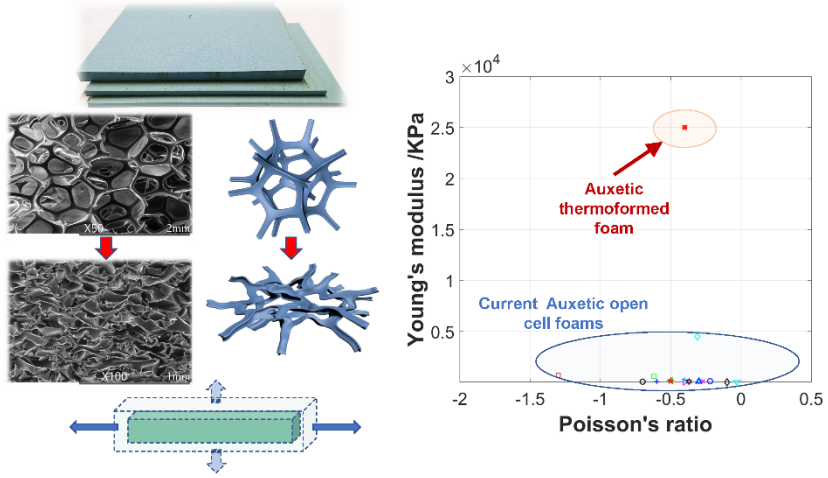

Keyword: Auxetic, thermoformed foam, negative Poisson' s ratio, modulus, loss factor

*Corresponding authors: Zhang, Q. (qicheng.zhang@bristol.ac.uk) and Peng, H-X. (hxpengwork@zju.edu.cn)

† Authors contributed equally to the present work

List of Symbols

a Width of specimen
b Length of specimen
E_t Tangent modulus
E_l Loss modulus
h Height of specimen
TF Thermoformed foam
ε_T Maximum tensile strain
ε_C Maximum compressive strain
η Loss factor
ν_{xy} Poisson' s ratio, when loading along direction y

1. Introduction

Auxetic materials are a class of metamaterials exhibiting negative Poisson' s ratio[1,2]. The counter-intuitive deformation of auxetic materials leads to some special multifunctional properties such as resistance to high shear deformation [3,4], indentation resistance[5], improved fracture resistance[6,7], synclastic behavior[8,9], variable permeability[10] and high energy absorption capacity[11-17]. Therefore, auxetic materials have significant potential in several applications ranging from personal protective equipment[16], noise reduction[17-19], cushioning[20], aircraft seats[21,22] and garment textiles[23].

Large subsets of auxetic metamaterials and structures are reported in scientific literature. Auxetic polymeric foams are amongst the most successful examples of negative Poisson' s ratio materials physically produced, due to their relative straightforwardness of manufacturing and general good mechanical properties[24]. The manufacturing of auxetic foams was first developed by Lakes in 1987[25] and then modified by other researchers[15,26-30]. The classical manufacturing procedure to transform conventional open cell polymeric foams into auxetic versions typically includes the following steps: volumetric compression, heating (annealing), cooling and relaxation[15,25,29]. The volumetric compression step, usually carried out in a mold, is used to obtain the typical auxetic re-entrant pores microstructure inside the foams through buckling of cell ribs; and then the re-entrant pore shape is fixed via thermoforming with the following heating and cooling procedure[31-33]. Other manufacturing processes involve the use of compressed carbon dioxide[34] or solvents[35] to replace the high temperature thermoforming procedure. Some of the Authors of this work have used vacuum bags to replace the rigid mould[36].

Different manufacturing and material parameters can affect the properties of auxetic foams, such as the pristine (conventional Poisson' s ratio) foam cell size, the composition of the materials, volumetric compression, heating temperatures and time [24]. Amongst them, the volumetric compression ratio has been considered as one of the most important parameters[15,37,38]. The volumetric compression ratio values used in the majority of publications available from scientific literature range between 2 and 10 [24,28,37,39], except for some trials that have adopted larger ratios reaching 19 [15,40]. The properties of auxetic foams can greatly determine their applications. Stiffness is one of the parameters used to assess indentation

resistance for the design of cushion/seats[5] and hysteresis is an indication of energy absorption for quasi-static loading[4,41]. Higher auxeticity can enhance the indentation resistance performance[5,42], impact energy absorption capability[41,43] and synclastic behavior[44], which are essential for the application of auxetic foams.

In Fig. 1, we present a diagram illustrating the distribution of the Poisson' s ratio and Young' s modulus of auxetic polymeric foams present in scientific literature. The modulus and Poisson' s ratios shown in Fig. 1 include both compressive and tensile results and are all based on small deformations (within 20% strain) because the modulus in these foams tends to increase nonlinearly at higher strains[28,45]. Values of the Poisson' s ratio appear to be mainly distributed between -1.5 and 0, while the modulus is within 20kPa and 700kPa. The auxetic foams currently available appear therefore to be very compliant. The only exception seems to be the negative Poisson' s ratio foam produced by Mohsenizadeh, et al.[28], with a modulus reaching 4.5 MPa and a negative Poisson' s ratio of -0.3 at 10% strain. That foam was however tested under compression only on small size specimens, and stiffer closed-cell foam with modulus of ~4MPa has been used as the pristine baseline. Other auxetic polymer cellular metamaterials with significant stiffness have also been developed by Rueger, et al. (0.9MPa)[46] and Li, et al. (100MPa predicated by simulation)[47]; those lattice materials had however complicated internal structures that would need to be manufactured by using 3D printing methods. There are also some studies about the loss factors of auxetic foams to describe the damping property in quasi-static tests. Bianchi et al.[15] have observed loss factors between 2.7% and 4.7% in mould-based thermoformed auxetic foams, although the loss factor was determined using the tangent loss concept. Cheng et al.[4] have measured in three-point bending tests with loss factors between 4.7% and 5.3%. Rueger and Lakes[48] have measured the loss factors of reticulated negative Poisson' s ratio open cell polyurethane foams ranging between 3.5% and 5.0%, using tanδ (equivalent to 4 times the definition of loss factor used here) as the parameter to describe the damping property. Those foams however possess lower densities (96 kgm^{-3}) and compressive stiffness (25 kPa).

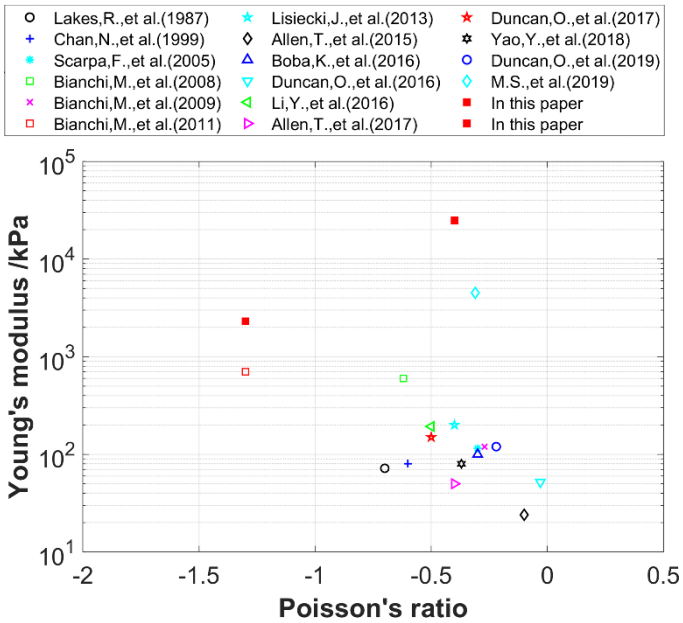

Fig. 1 Poisson' s ratio and Young' s modulus of auxetic foams in scientific literature. All moduli are calculated at small strains (within 20%).

In this work we aim to develop high-stiffness thermoformed auxetic foams by enhancing the manufacturing process previously developed by some of the Authors of this paper[36]. The production method involves the use of vacuum bags, pressure pumps and autoclave to perform the thermoforming procedure of open cell polyurethane (PU) foams. The auxetic foams produced in this work are quite dense and stiff. Both tensile and compression quasi-static tests (uniaxial and cyclic) have been performed to identify the Young' s modulus and Poisson' s ratio of the thermoformed foam from specimens cut along different directions from the same block originated by the production process. Foam samples are also trained (i.e., subjected to specified tensile strains to further relax the thermoformed samples). The effects of the thickness of the specimens and maximum tensile training strain are also evaluated. Because of the specific porous configurations of these foams, the properties can also be affected by other parameters such as the foam cell size of the pristine foam, the composition of the core material and the volumetric compression used. A complete exploration of the manufacturing design space for these foams is however beyond the scope of this paper.

As shown in Fig. 1, the tensile modulus and Poisson' s ratio of the auxetic foams presented in this work can reach 25MPa and -0.4, with -1.3 achieved for lower thickness, with a loss factor ranging between 2% and 6%. These foams therefore exhibit a remarkable mechanical performance in terms of stiffness and auxeticity perspectives compared to other auxetic foams in scientific literature, although the auxetic behavior is present in one plane only.

2. Manufacturing process of the thermoformed auxetic foam

The manufacturing procedure of the auxetic thermoformed foam (TF) is presented in Fig. 2, based on a methodology previously developed by Bianchi et al.[36], with variations mainly focused on the profile temperature and the configuration of the mould. The pristine open-cell polyurethane foam is supplied by the SM Upholstery Ltd., with the density of 28.7kg/m^3 and the pore linear density of 1102-1378/m. The pristine foam pad with length and width of 500mm×400mm is wrapped with a FEP release film and a white polyester non-woven breather blanket. The wrapped foam is then placed on a large steel plate with an aluminum cover plate on top. The foam-breather-plate assembly is then placed in an air-tight bag, made of a flexible membrane with double side sticky tape sealed around. A vacuum pump is then used to reduce the pressure inside the bag with a vacuum nozzle connecting the pump to the bag. The bag is then subjected to a technical vacuum with pressure lower than 0.7 bar. The aluminum cover plate on top is drawn to the bottom steel plate as the pressure inside the bag decreases and the foam therefore collapses to a smaller thickness. The top and bottom plates are used to keep the flat shape of the top and bottom surfaces of the foam after the collapse of the pores. The compression of the foam cells and the deformation of their ribs appear to be highly uniform across the thickness of the foam pad, resulting in a substantially homogeneous re-entrant cell structure throughout the foam panel. The top cover plate used in this work allows to obtain TF pads with large thickness. In comparison, no TF with thickness higher than 5mm has been successfully made before by purely following the process in[36] because the top breather and the membrane would be severely distorted and wrinkled during the vacuuming of the foam pads, especially when the latter possess high thickness values.

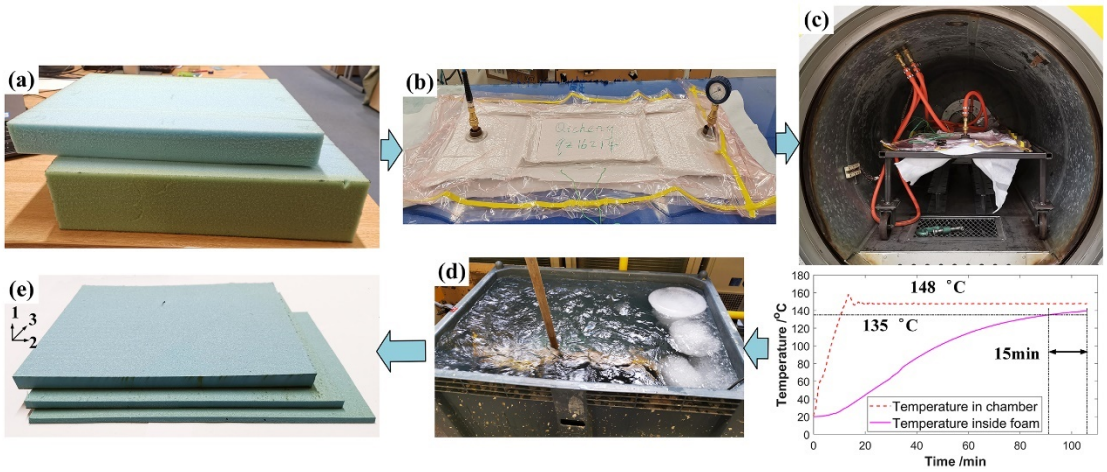

Fig. 2 Manufacturing procedure of the thermoformed auxetic foam. (a) pristine foams, (b) bag sealing and vacuum, (c) heating in autoclave with the temperature profile, (d) cooling in iced water and (5) obtained thermoformed auxetic foam pads

The foam in the vacuum bag is then placed in an autoclave at a pressure of 219kPa. The autoclave chamber is then heated up to 148°C with a thermocouple inserted inside the foam and another one installed in the autoclave to observe the temperature. The temperature curves inside the chamber and the foam are shown in Fig. 2 (c). The temperature inside the foam increases slower than the ambient temperature because of the thermal insulation of the foam and the breather. The foam temperature tends to plateau when getting closer to the one of the environments at steady state. The heating procedure is terminated 15 min after the foam temperature reaches 135°C, which is higher than the glass transition temperature of the foam (114°C [49]). The whole assembly (bagged foams with plates) is then removed from the autoclave and swiftly immersed in iced water at 3°C for 20 minutes. The sealing bag and the breather are then detached, and the curved outer rim of the foam pad cut away to obtain a thermoformed foam plate with homogeneous thickness. Compared with the original work from Bianchi et al.[36], the heating process used here is slower and provides a more homogeneous annealing of the foam pad. Thus the foam is thermoformed in a more uniform manner and does not show evident thickness increases after manufacturing compared with the ~30% thickness increment purely using the method of Bianchi et al.[36].

The vacuum manufacturing method provides an earlier and more uniformly distributed triggering of the buckling of the foam ribs. This is opposite to what happens when using a classical mould compression manufacturing method[15]; the buckling of the ribs first occurs on the boundary of the pristine foam block and then spreads into the inner parts as the compression force increases. The TF presented in the current work is manufactured using a higher compression ratio and presented homogeneous inner structures due to the vacuum manufacturing method. The denser inner configuration of the foam and the more stable and uniform thermoforming method result in the higher stiffness of the final porous material.

Three patches of foam plates with different thicknesses have been manufactured using the same method introduced above. The thicknesses of the pristine foam and the TF case are listed in Table 1. The thickness of the thermoformed foam is roughly 10% of the pristine one,

resulting in a high-density TF. The measured densities of the TF pads with different thicknesses are listed in Table 1. Those densities are approximately 10 times those of the pristine foam (28.7kg/m^3). The density of the thicker TF pad is slightly larger than the thinner one. One reason behind this is that the pristine foam block tends to shrink during vacuum mainly along the axial direction (direction 1) and also (albeit slightly) along the lateral direction (direction 2, 3 - see Fig. 2(b)). As the thickness increases, the lateral shrinkage becomes more obvious. The compression ratio of the batch #2 pad is also slightly higher than the one used for the other two batches.

The temperature inside the foam pad increases slower with the increasing thickness because of the better thermal insulation provided by the thicker foam. The criteria to terminate the thermoforming process is the temperature reached inside the foam pad. As the thickness increases from 5mm to 9mm and 15mm, the total heating time increases from 67 mins to 80 mins and 105 mins (Table 1). This implies that the outer part of the thicker TF is subjected to longer heating times to ensure an adequate heating of the inner part, which is essential for a more uniform thermoforming.

Table 1 Thickness of foams in different batches

	Batch 1	Batch 2	Batch 3
Thickness of pristine foam	49mm	101mm	153mm
Thickness of TF	5.0mm	9.1mm	15.5mm
Density (kg/m^3)	282.4	315.5	314.2
Total heating time (min)	67	80	105

3. Configuration of the specimens

Specimens with different sizes and orientations have been cut from the production slab to study the mechanical properties of the TF. Three different types of specimens have been produced (Fig. 3 and Table 2). The type T long rectangle specimens are used for tensile tests, with length and width of 150×20mm for 3 different thicknesses. Two samples have been cut along the 2-direction and one along the 3-direction to compare the transverse properties. The type C cubic specimens with edge length of ~15mm have been used for compression tests loading along different directions. Initial tests showed that the mechanical performance of the foam was sensitive to previous tensile loading history of the samples. The tensile loading can lead to the detachment and break of microstructures inside the TF, working similarly to relaxation[18,26] or stretching[36] processes described by other researchers. Type P specimens have been therefore cut from the long rectangle specimens after tensile training with different strains. The training process of each specimen has been repeated 5 times to reach a stable state of the material. Type P specimens (length and width 30×30mm for the 3 batches of thicknesses) have been tested under compression along direction 1.

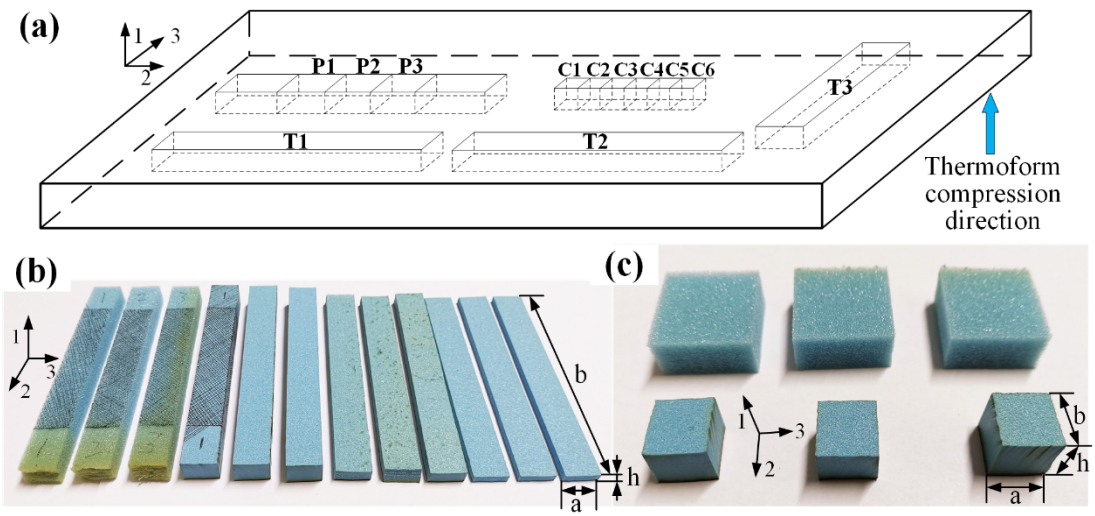

Fig. 3 Orientation of the specimens in the foam slab (a) and the specimens for tensile test (b) and compression test (c)

Table 2 Sizes of different specimens. Each specimen has 3 parallel samples

Test type	Specimen type		a /mm	b /mm	h /mm
Tensile test	Pristine foam		20	150	15.1
	TF-5mm Batch 1		20	150	5.0
	TF-9mm Batch 2		20	150	9.1
	TF-15mm Batch 3		20	150	15.1
Compression test 1: different loading directions	Pristine foam		30	30	15.1
	TF-15mm, in direction 1		15.2	15.4	15.5
	TF-15mm, in direction 2		15.3	15.5	15.4
Compression test 2: specimens with different tensile training strains	TF-5mm	0% tension	30	30	5
		20% tension	30	30	5
	TF-9mm	0% tension	30	30	9.1
		5% tension	30	30	9.1
		10% tension	30	30	9.1
		15% tension	30	30	9.1
		20% tension	30	30	9.1
	TF-15mm	0% tension	30	30	15.5
		20% tension	30	30	15.5

4. Microstructural characteristics of the thermoformed auxetic foam

Scanning electron microscopy (SEM, using the Hitachi TM3030plus tabletop microscope) images of the pristine foam and the TF are shown in Fig. 4 and Fig. 5 respectively. Open cell

PU foams are produced out of reactors, with the foam cells tending to align along the rise direction. This is also valid for large slabs produced at industrial scale, so the resulting foam is slightly anisotropic. As observed in Fig. 4, there is no noticeable structural difference along different directions, indicating the anisotropy of pristine foam is minimal. Also, because the foam pads for thermoforming and the pristine foam specimens are all cut along the same orientation, any slight deviation of the cutting along different directions should not significantly affect the measured data. The open-cell pristine foam is obviously reticulated with membranes present between neighboring cells. The average diameter of the cell structure is ~500μm, while the average diameter of the ribs with a triangular cross section is ~50μm.

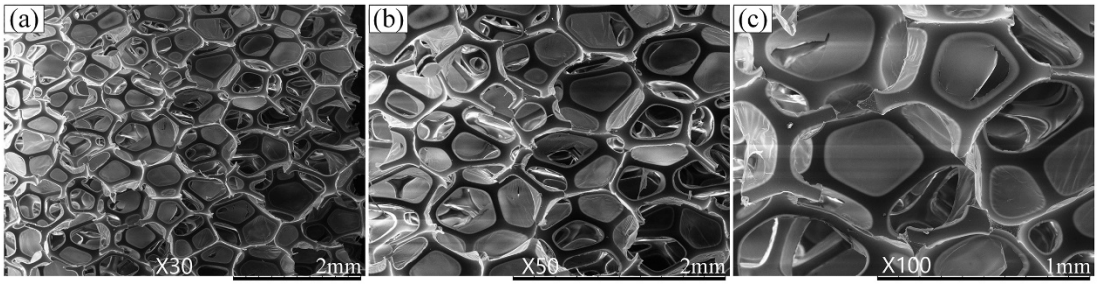

Fig. 4 SEM images of the pristine foam along direction 1: (a) x30, (b) x50 and (c) x100

The microstructure of the TF with thickness of 9mm along the compression direction (direction 1) and transverse directions (directions 2 or 3) are quite different (Fig. 5). This indicates the presence of transverse isotropy of the TF produced. The SEM images of foams cut along directions 2 and 3 are quite similar, so only the images along the directions 1 and 2 are shown in Fig. 5. The microstructures observed along direction 1 shows the partially original reticulated structure with kinks along the ribs, exhibiting the typical re-entrant configuration of auxetic foams [32,36,50]. The microstructure configuration related to direction 2 is more elongated and compressed compared to the one from direction 1. The collapsed ribs are interconnected and contact each other due to the predominant one-dimensional compression induced by the vacuum pump. It is possible to observe from the SEMs along the 1 and 2 directions that the tomographic inner pore structures of the TF exhibit a strong directionality and overall transverse isotropic characteristics of elongated semi-reticulated configuration. The SEM images in Fig. 5 (g)-(i) are related to the boundary (the surfaces close to the top and bottom plates) of the TF specimens. The pictures show no special characteristics at the boundary area compared with the microstructures inside the specimen (Fig. 5 (d)-(f)). The direct contact with the plates and the different temperature history due to the thermal insulation of the foam during manufacturing does not therefore introduce any special effect on the microstructures of the foam boundary. As discussed in Section 2, the thickness of the foam pad could affect the lateral shrinkage during vacuuming and therefore affect the topology of the microstructures inside the TF. However, the differences are very small and no visible changes can be distinguished in the SEM figures of TF with different thicknesses due to the complexity of the interconnected microstructures.

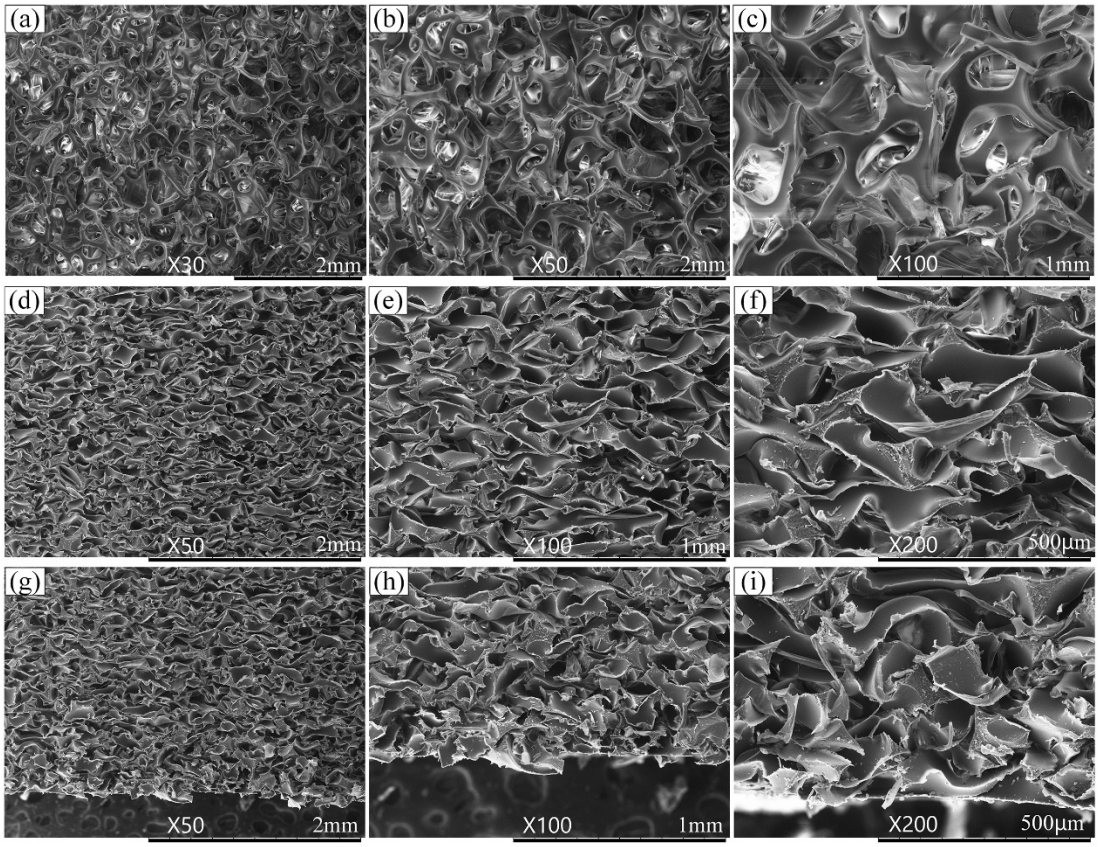

Fig. 5 SEM images of the thermoformed auxetic foam with different gains: (a) x30, (b) x50 and (c) x100 are all along direction 1; (d) x50, (e) x100 and (f) x200 are all along direction 2; (g) x50, (h) x100 and (i) x200 are boundaries of the thermoformed auxetic foam specimen along direction 2

Schematics of the 3D cell structures of the pristine foam and the TF based on the SEM observations are shown in Fig. 6. The pristine foam cell can be simplified as a dodecahedron. After the compression occurring during thermoforming along the direction 1, the foam cell reduces its height and tends to become flat without any significant change in terms of length and width; this leads to a lattice configuration with a significant anisotropy. The foam ribs with projections oriented along the 1-direction buckle and form re-entrant structures that provide the auxetic behavior of the TF[25,31]. The material is therefore able to expand along the direction 1 when tensioned along the 2 or 3 directions. The thermoforming compression ratio of the TF is ~10% and this leads to a quite dense foams with the buckle ribs almost contacting each other. It should also be noticed that the foam pad also shrinks slightly along direction 2 and 3 during vacuuming especially when the thickness is large. The slight lateral shrinkage could result in some re-entrant configurations of the cells along directions 2 and 3; which could slightly affect the mechanical properties of the TF with different thicknesses.

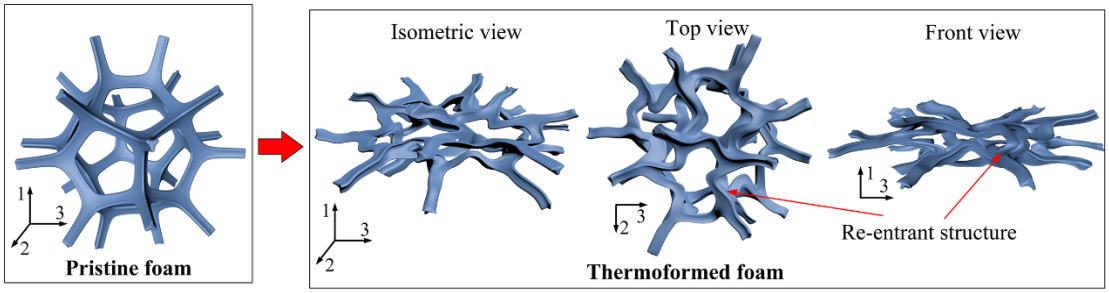

Fig. 6 Cell structures of the pristine foam and thermoformed foam

5. Test rig and methodology

The rig for the quasi-static tests is shown in Fig. 7. Both tensile and compression tests were carried out using a single column tabletop testing system (Instron, type 3343) with a 1kN force sensor (Instron, model 2519-105). A dual-camera video system (iMETRUM Limited, camera type CAM 13) has been used to measure the Poisson' s ratio and the axial strain along two orthogonal lateral directions. Nominal strain and stress are used to calculate the modulus of the material during the tests. The Poisson' s ratio is defined as $\nu_{xy}=-\varepsilon_y/\varepsilon_x$, where ε_y and ε_x are the nominal strains along transverse and axial loading directions respectively[4]. The layout of the Poisson' s ratio measurement is illustrated in Fig. 7 (c) and (d). Three values of the Poisson' s ratio have been measured on each lateral surface for average; no noticeable deviation has been observed among those values during the actual test. The distance between points related to the axial strain measurement is 50% of the specimen length during the tensile test and 80% of the specimen height in compression. The distance between points for the transverse strain measurements is 80% of the specimen width for both tensile and compression tests. The residual strains in the axial and transverse directions of the specimen should be eliminated when calibrating the Poisson' s ratio directly measured from a video gauge. The Poisson' s ratio is defined starting from a material subjected to loading from an undeformed state; the Poisson' s ratio of foams could vary with the deformation, especially at large strains[51]. The maximum strain used in this work is ~15% after excluding the residual strain, which is significantly lower than the 500% used in reference[51]. The reduction of Poisson' s ratio affected by the 15% strain deformation is acceptable and does not affect the main conclusions of this paper.

To reduce measurement errors induced by boundary and Saint-Venant effects, only axial strains belonging to the 50% middle part of the specimen are measured by using a video gauge to determine the tensile modulus (Fig. 7 (c)). In compression, the buckling of the ribs belonging to the pristine foam cells first occurs near the top and bottom boundaries of the specimens, and then spread into the middle parts of the samples[45]. The displacement of the top compression plate is therefore used to calculate the axial compressive strain of the whole specimen to determine the compressive modulus. For the Poisson' s ratio calculations, the axial and horizontal strains of the 80% middle part of the specimens are measured by video gauge (Fig. 7 (d)). For the pristine foams, the axial strain measured from the 80% middle part by video gauge is however slightly smaller than the total deformation at small strains when the buckling of the foam ribs first occurs only near the top and bottom boundaries of the specimens. As the buckling spreads from the boundaries to the inner parts, the deviation between strains from the video gauge and the top plate displacement is almost unnoticeable.

No obvious boundary effect is observed on the TF specimens during compression, thus the axial strain measuring methods appear to have negligible effects.

Preliminary tests have shown that the modulus decreases with the loading rate and gradually reaches a constant value when the loading rate reduces to ~3mm/min. The tests have therefore been carried out in displacement control mode with a loading rate of 2mm/min, which is deemed sufficient to approximate a quasi-static testing regime. A preload of 0.5N has been applied to obtain a more stable initial testing state. Due to the Mullins effect[52], the first few cyclic loops during the tests show some obvious differences and the mechanical property of the TF tends to show some stability after four loading cycles. A five loading-unloading cyclic loops test has been therefore applied to each specimen and only the 5th loop was used to evaluate the properties of the material[53]. The loss factor is calculated from the tested hysteretic loops and defined as $\eta = \Delta W/(2\pi U)$, where ΔW is the dissipated energy within one hysteretic loop and U is the corresponding elastic energy stored in the material[53,54]. The loss modulus can be defined as $E_l = E_t \cdot \eta$ and represents the capacity of absorbing mechanical energy [54,55].

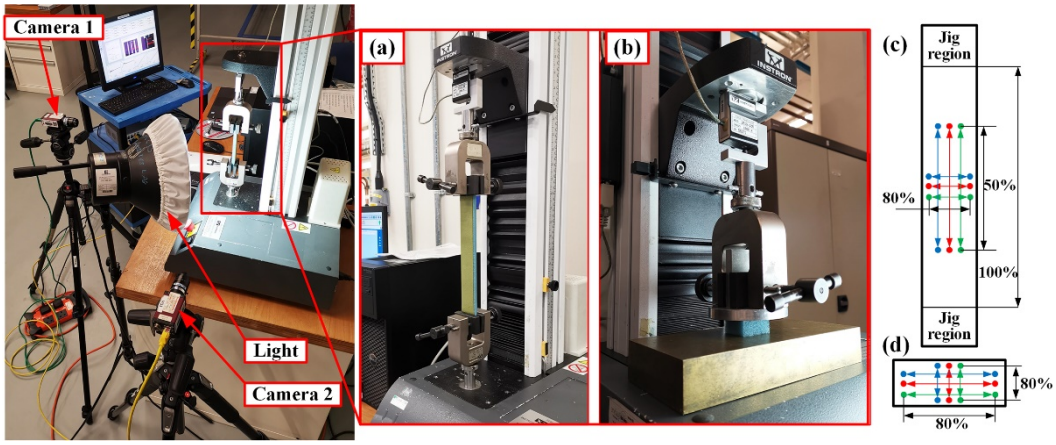

Fig. 7 Test rig of quasi static experiments and the layout of Poisson' s ratio measurement: (a), (c) tensile test and (b), (d) compression test

6. Tensile tests results

The typical hysteretic loops from the tensile tests for the TF and the pristine foam specimens with 15 mm of thickness are compared in Fig. 8. At least 3 parallel specimens with same parameters were tested and the deviation among these parallel specimens is quite small, as shown by the error bars present in Fig. 9 and Fig. 10. The testing procedure applied to each specimen involves the sequential application of a tensile loading for 7 times with different maximum strains ε_T (from 5%-1st, 10%-1st, 15%-1st to 20%-1st and then reducing to 15%-2nd, 10%-2nd and 5%-2nd; the 1st here indicates the first time testing has been performed with this strain; the 2nd here is related to the second time testing with this strain has been carried out and the specimen has also undergone tests with higher strains previously). Five loops of cyclic loading and unloading were conducted for each maximum strain tensile test and only the last loop was used for comparison. A residual deformation of the specimen can be observed after tensile test, thus the 5th hysteretic loops always start from a residual strain and end at a nominal strain of 5%, 10%, 15% and 20%[53]. After shifting the hysteretic loops to start at

the origin of the graph coordinates the maximum strains have been reduced from nominal values to 3%, 7%, 10% and 14% respectively (Fig. 8). A similar adjustment has also been observed for the compression tests (Fig. 11 and Fig. 14). No noticeable deviations of the test results between specimens cut along the 2 and 3-directions (Fig. 3) have been observed, indicating a good degree of transverse isotropy of the TF. It is possible to observe from Fig. 8 (a) that the slope of the strain-stress curves from loading decreases monotonously as ε_T increases from 5% to 20% and stays unchanged as ε_T decreases from 20% to 5%. This implies that the tensile deformation applied reduces the stiffness of the foam and the same stiffness remains almost constant after the tensile training. This phenomenon is similar to the Mullins effect in rubbers[52]. In comparison, the stiffness of the pristine foam remains constant as the maximum tensile strain increases (Fig. 8 (b)). The effect of the ε_T strain on the TF will be discussed in detail when commenting Fig. 10.

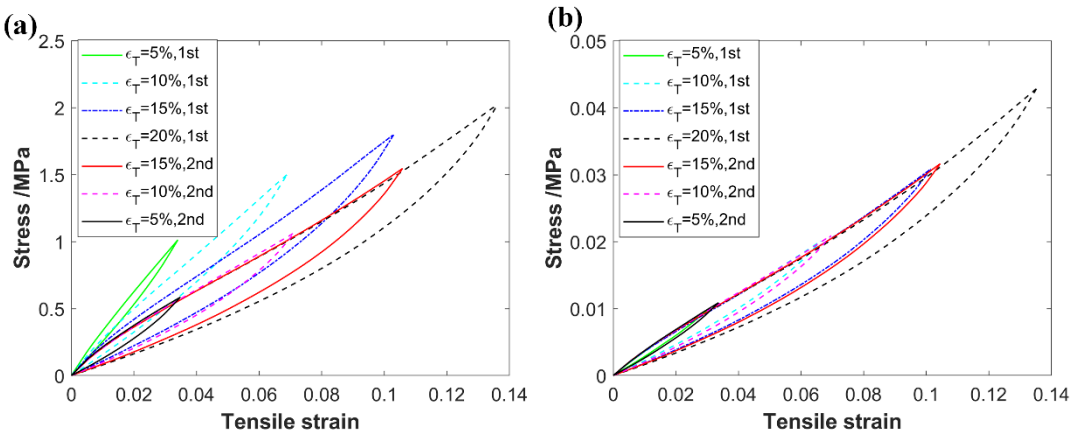

Fig. 8 Hysteretic loops of the TF (a) and pristine foam (b) with 15 mm thickness. The foams have been tested with different maximum tensile strains

The tangent modulus and Poisson' s ratio of the foam with a maximum 20% tensile strain are shown in Fig. 9. The tangent modulus E_{t2} of the TFs decrease obviously first with the strain until ~2%, with a stable plateau up to ~8% strain and final gentle increase. The strain-modulus curves of the specimens with different thicknesses have similar variations. At small strains, the E_{t2} of the TF-5mm reduces by 40% from ~2MPa to ~1.2MPa; the TF-9mm reduces by 48% from ~8.6MPa to ~4.5MPa; the TF-15mm reduces by 44% from ~25MPa to ~13.1MPa and the pristine foam reduces by 35% from ~0.4MPa to ~0.26MPa. The first decrease of the E_{t2} modulus with increasing strain is mainly caused by the behavior of the polyurethane material at small strains due to the Mullins effect in cyclic loading[52,56]. The Mullins effect is a particular aspect of the mechanical response of rubber and polymer in which the stress–strain curve depends on the maximum loading previously encountered. At times, when the load is less than a prior maximum, nonlinear viscoelastic behaviour prevails. As mentioned above, five loading-unloading cyclic loops are performed for each testing condition, and only the 5th loop is used for further data processing and comparison. During the 1st loading at a maximum strain of 20%, the deformation causes small changes to the microstructure of the bulk polyurethane and results in a slight nonlinear behavior of the elastomer at small strains in the following cyclic loops[56]. Although the maximum strain of the TF specimen is only 20%, the local strain of the ribs could be larger because some of the ribs are also under bending, thus the

influence of the Mullins effect is not negligible. The value of E_{t2} at the plateau however increases significantly from ~1.2MPa to ~4.5MPa and ~13.1MPa as the specimen thickness increases from 5mm, 9mm to 15mm, compared with the 0.26MPa modulus of pristine foam. In comparison, the specific moduli (defined as modulus over density) of the pristine foam and the TF-5mm, TF-9mm and TF-15mm specimens are 9.1, 4.3, 14.3 and 41.7 kPa/(kg/m^3) respectively. The specific moduli of the TF-9mm and TF-15mm also increase significantly compared to the pristine foam.

The Poisson' s ratios ν_{23} of the TF is positive between 0.25 and 0.45 and smaller than the one of the pristine foam (Fig. 9 (b)). The ν_{23} varies slightly with the tensile strain and declines for larger thickness values of the specimen. In comparison, the Poisson' s ratio ν_{21} of the TF remains negative within a range from -1.3 to -0.4 as shown in Fig. 9 (c). The ν_{21} of specimens with thickness of 15mm and 9mm are quite similar and both remain constant around -0.4. The thinner 5mm specimen exhibits a larger auxeticity, as the ν_{21} increases from -1.3 to -1.0 with the strain. The auxeticity in the 1-2 plane is caused by the re-entrant microstructures provided by the buckled ribs (Fig. 5 and Fig. 6). In comparison, the convexity of the cell microstructures in the 2-3 plane is limited (Fig. 5 and Fig. 6) and that leads to positive values for ν_{23}. It should also be noticed that the ν_{21} and ν_{23} of the pristine foams are all close to 0.6, exceeding the theoretical range of Poisson' s ratio of isotropic materials[25,57,58]. As explained before, this is because the pristine foam is slightly anisotropic due to the manufacturing process. In reality the Poisson' s ratio of conventional foams has been already measured with values higher than 0.5 (0.5-0.7[45,59,60]).

The thickness-dependent properties of the TF are caused by the deformation mechanism and the manufacturing. The re-entrant microstructures inside the TF could expand along the direction 1 when subjected to transverse tension in the 2-3 plane, leading to an increase of specimen thickness and the partial detachment of the ribs of the elongated pores. The consequent reduction of the convolutedness of the cells microstructures and numbers of ribs sticking together could lead to lower stiffness of the TF material. With higher thickness, the inner microstructures of the TF specimen are more difficult to expand and detach along the 1-direction when loading along the direction 2, due to the constraint offered by the outer layer foam materials. Besides, a layer of damaged cells at the surface is contributing to the compliance and the role of the surface becomes less pronounced as the thickness increases. Thus, the stiffness is larger and the auxetic phenomenon is less evident for thick TF specimens. Also, the more uniform and homogeneous thermoformed microstructure present in thicker specimens could also favor an increase of stiffness. The slight shrinkage of the foam block in 2-3 plane during manufacturing described in Section 2 increases with the thickness of the pad; this results in cells with higher convexity in the 2-3 plane. The ν_{23} therefore decreases with the thickness of the specimen and remains always positive. The ν_{21} values of the TF-9mm and TF-15mm specimens are quite similar and this contradicts the analysis that the auxeticity decreases with increasing thickness. This however may be explained by the difference in compression ratio used during manufacturing (see Table 1).

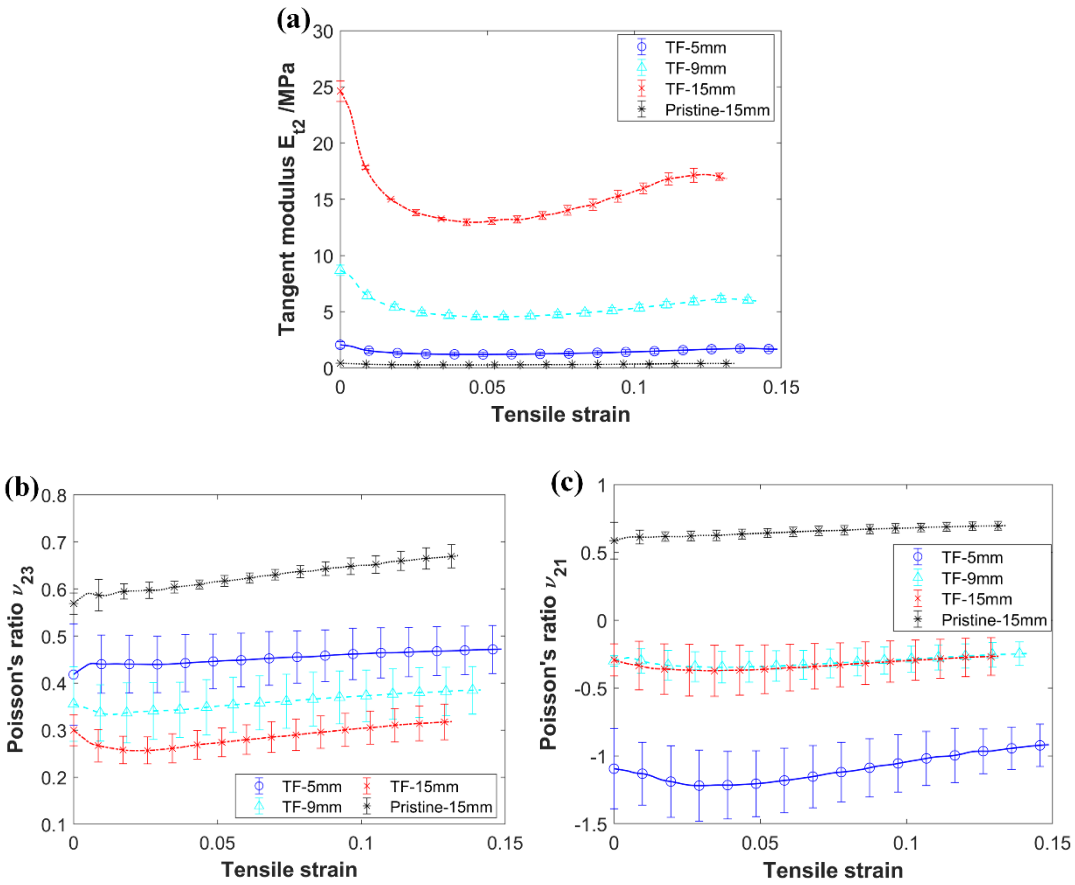

Fig. 9 Tangent moduli (a), Poisson' s ratio ν_{23} (b) and ν_{21} (c) versus strain for the TF specimens with different thicknesses subjected to a maximum tensile strain of 20%

The effect of the maximum tensile strain ε_T on the TF foam properties has been evaluated at 3% strain of each strain-property curve. It is evident from inspecting Fig. 10 (a) that the tangent modulus E_{t2} reduces with the maximum tensile strain ε_T, while the loss factor η_2 increases from ~0.02 to ~0.05 with it. The increase of specimen thickness will significantly enhance the E_{t2} with little effect on the η_2. The loss modulus E_{l2}, equals to $E_{t2}\cdot\eta_2$, remains almost constant with ε_T because of the increase of the tangent (storage) modulus E_{t2} and the decrease of η_2 (Fig. 10 (b)). The loss modulus E_{l2} rises from ~0.06MPa, ~0.25MPa to ~0.65MPa as the specimen thickness of TF increases (from 5mm, 9mm to 15mm). Those loss modulus values are always significantly higher than the ~8kPa of the pristine foam. In Fig. 10 (c), the Poisson' s ratio ν_{23} of different TF specimens is positive and with slight variations around 0.3; and this Poisson' s ratio is smaller than the ~0.6 value of the pristine foam. On the contrary, the negative ν_{21} of TFs decrease significantly with ε_T, especially in the case of the thin 5mm TF specimen which reduces from -0.33 to -1.3 compared with the thicker TFs (from ~0 to -0.4). The lower stiffness and enhanced auxeticity of the TF after tension are mainly caused by the detachment of the intertwined ribs between partial membranes and the break of the weaker cell ribs inside the TF, resulting in more dominant re-entrant microstructures, larger micro deformation and more evident sliding between ribs under external loading which leads to higher loss factors. The Mullins effect of the polymer material also plays a partial role in reducing the modulus of the foam after a maximum strain history.[52]

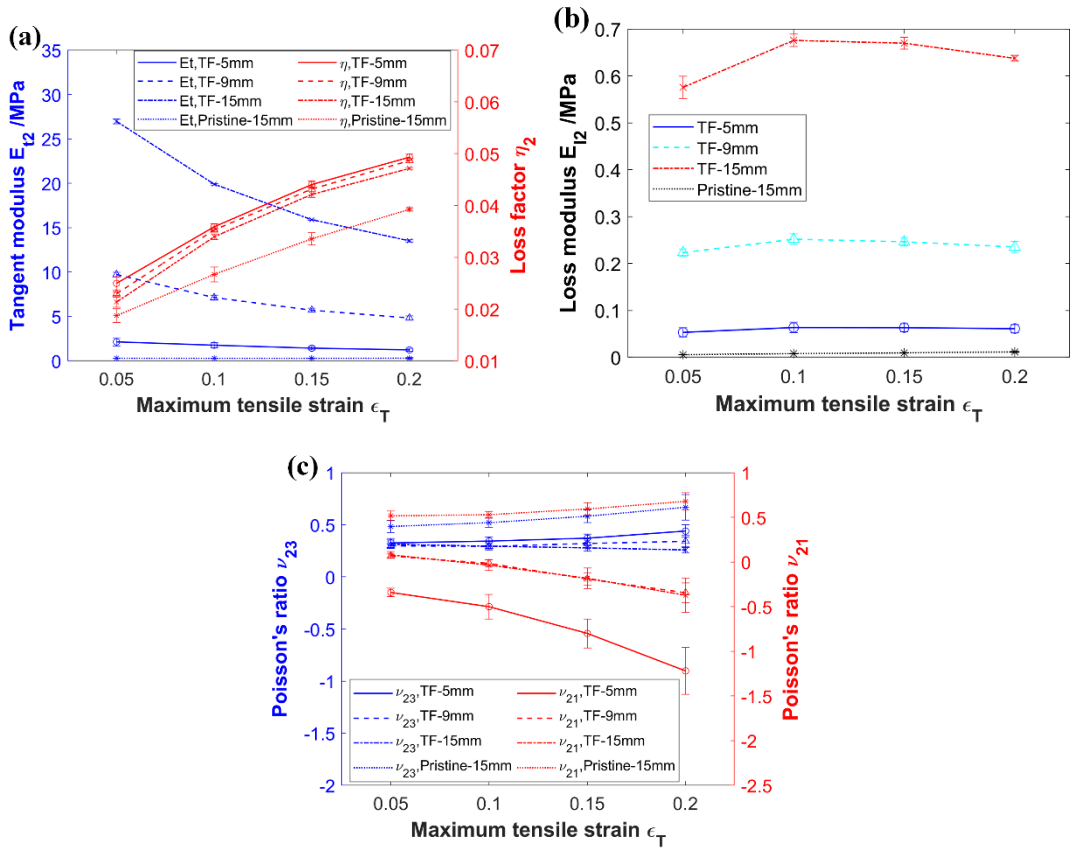

Fig. 10 Properties at 3% strain for specimens tested at different maximum tensile strains. Tangent modulus and loss factor (a), loss modulus(b) and Poisson' s ratios (c)

7. Compression tests with loading along different directions

The hysteretic loops of different foam specimens under compression are shown in Fig. 11. The TF is compressed along the thermocompression direction 1 and transverse direction 2, respectively. The loading procedures are quite similar to the ones operated on the tensile tests, and those include 7 series of compression loading with different maximum strains ε_C on each specimen. Similar to the results observed during the tensile tests, the slopes of the strain-stress curves of the TF foams in compression decrease monotonously as ε_C increases from 5% to 20%. The slopes also tend to overlap each other as ε_C reduces from 20% to 5%.

The compression loading appears to reduce the stiffness of the pristine foam (Fig. 11 (c)), opposite to the no effect provided by tension (Fig. 8 (b)). This is because the tensile and compressive behaviors of the pristine foam are quite different. When subjected to tensile loading, the ribs inside the pristine foam are mainly under tension and bending without buckling. Thus, the deformation of the ribs is elastic, linear and recoverable[45]. On the opposite, in compression the ribs inside the specimen are mainly under compression and bending and can easily reach buckling. The buckling of foam ribs first occurs at the top and bottom boundaries of the specimen and then spread into the middle parts of the sample as the compression force increases[45]. When buckling happens, the foam ribs undertake high local deformation and strain, exceeding the elastic limit of the polyurethane polymer.

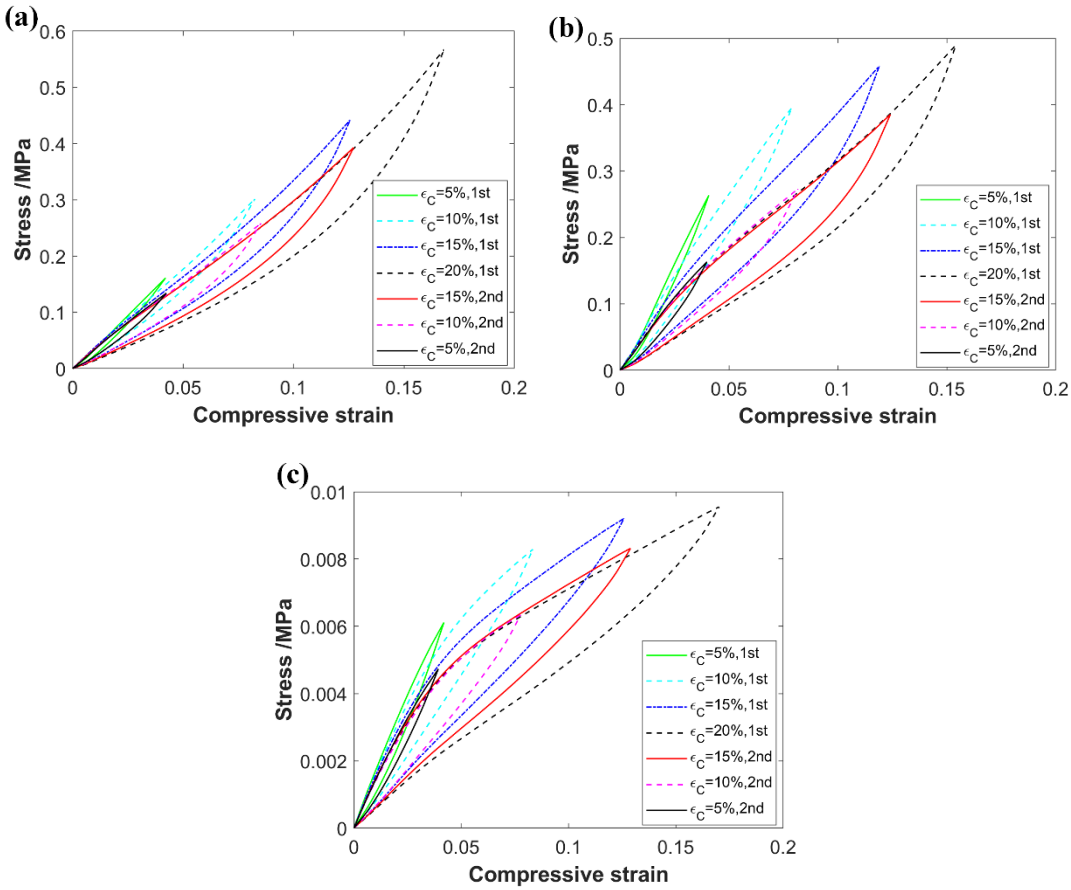

Fig. 11 Hysteretic loops of samples tested with different maximum compressive strains. TFs along direction 1 (a) and 2 (b), and the pristine foam (c)

The tangent modulus and Poisson' s ratio of the foam in compression up to a maximum nominal strain of the 20% (now 17%) are shown in Fig. 12. The moduli E_{t1} and E_{t2} of the TFs range between 2.6MPa and 4.8MPa, significantly higher than the pristine foam. The E_{t1} decreases first within 2% strain and then increases slowly after a plateau. The large standard deviations of E_{t2} at small strains (within 2%) are caused by the uneven and nonparallel contact surface between the specimen top surface and the compression plate of the machine. Thus, ignoring the results within 2% strain, the E_{t2} reduces with strain until ~6% and then increases slowly after a plateau. The reduction of the E_{t1} modulus at small strains is due to the behavior of the polyurethane caused by the Mullins effect under cyclic loading[56], similarly to the tensile tests in Fig. 9 (a). The final increase is caused by the densification of the inner cell structures. Apart from the nonlinearity of the polyurethane, the reduction of E_{t2} within much larger strains (~6%) is also caused by the buckling of the convoluted ribs inside the TF. This is because the ribs of cells mainly orientate on the 2-3 plane (Fig. 5 and Fig. 6), and this could favor the reaching of buckling under compression.

The Poisson' s ratios of TF under compression in Fig. 12 (b) are all positive, showing no auxeticity. When loading along the 1-direction, the ν_{12} and ν_{13} ratios of the TF vary slightly with the strain and remain stable around ~0.05. The low values of the Poisson' s ratios ν_{12} and ν_{13} in compression are mainly caused by the re-entrant and elongated densified microstructures of the TF in the 1-2 and 1-3 planes (Fig. 5 and Fig. 6). Aside for the case of

small strains lower than 2% discussed above, when loading along the 2-direction the values of ν_{21} and ν_{23} for the TF are almost constant at ~0.3. No obvious difference between compressive ν_{21} and ν_{23} values can be observed, and this is quite different from the results obtained from the tensile tests. This is because the microstructures are densely distributed in the inner parts of the foam (Fig. 5). The collapsed ribs are interconnected and contact each other due to the largely one-dimensional compression induced by the vacuum pump. When under tensile loading along the direction 2, the thickness along the 1-direction tends to increase due to the deformation of the re-entrant cell structure. The volume of the specimen increases as the density reduces. The contacts between ribs therefore reduce and the detachment of the convoluted unit cells along direction 1 can occur. The volume of the specimen decreases and the density increases when the samples are subjected to compression along the 2-direction. Therefore, the inner structures of the foam become denser and the ribs have tighter contacts, rather than being detached. The contacts between ribs prevent the re-entrant cell structures from shrinking along the direction 1. Thus, the specimen expands similarly along directions 1 and 3 when under compression along direction 2, similarly to the ν_{23} and ν_{21} cases. The Poisson's ratio of the pristine foam under compression decreases slightly from ~0.3 to ~0.19 with compressive strain, compared with the ~0.6 under tensile load from Fig. 9 (b) and (c). The different Poisson's ratio of the pristine foam in tensile and compressive loadings is caused by the different deformation mechanism of foam cells, as also observed by Chan et al.[45]

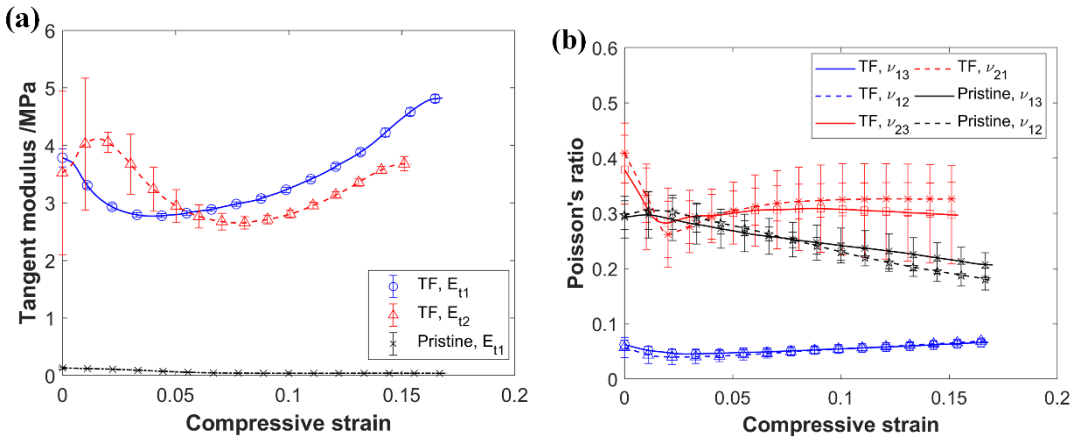

Fig. 12 Tangent modulus (a) and Poisson's ratio (b) versus strain along different loading directions

The effect of the maximum compressive strain ε_c on the TF foam properties along different directions has been evaluated at 3% strain of each strain-property curve. As shown in Fig. 13, the tangent modulus E_{t1} decreases by 24% from 3.7MPa to 2.8MPa, compared to a 46% reduction observed for E_{t2} (from 6.9MPa to 3.7MPa). The compression stiffness along the transverse direction 2 is significantly higher than the one observed on the thermocompression direction 1 because the foam ribs inside the TF mainly orientated in the 2-3 plane and are able to support higher loading along the transverse directions if the compressive load is not large enough for ribs to reach buckling. The relative deformation and sliding of contacts between ribs caused by the external loading could reduce the combination between convoluted ribs and result in damage and break, leading to the reduction of the E_t value. The

foam was compressed 90% along direction 1 and thermoformed during manufacturing, thus the TF is not very sensitive to the compressive training along this direction. As for what it concerns the compression along the 2-direction, the occurrence of large numbers of buckled ribs could only happen when the ε_C is high, providing a larger effect on the material. Thus, the reduction of the modulus caused by ε_C along the 2-direction is larger than along the 1-direction. Also in this case, Mullins effect plays a partial role in reducing the modulus of materials with previous maximum strain history.[52] The loss factors η of different foams all similarly increase from ~0.03 to ~0.05 as ε_C increases from 5% to 20%, mainly caused by the larger micro deformation and more evident sliding between intertwined ribs after compressive training.

The loss modulus E_{l2} increases from 0.16MPa to 0.21MPa with ε_C, compared with the smaller E_{l1} values (from 0.09MPa to 0.14MPa). Both E_{l1} and E_{l2} of the TF are significantly larger than the ~5kPa of the pristine foam and provide a greater energy absorption capability. When compressed along the 1-direction, the Poisson' s ratio ν_{12} and ν_{13} of the TF varies slightly around 0.06 with ε_C. On the contrary, the ν_{21} and ν_{23} values of the TF subjected to compression along direction 2 increases slightly from ~0.2 to ~0.3 with the maximum compressive strain ε_C. The Poisson' s ratio of the pristine foam is almost constant around 0.3, no matter which maximum compressive load has been applied.

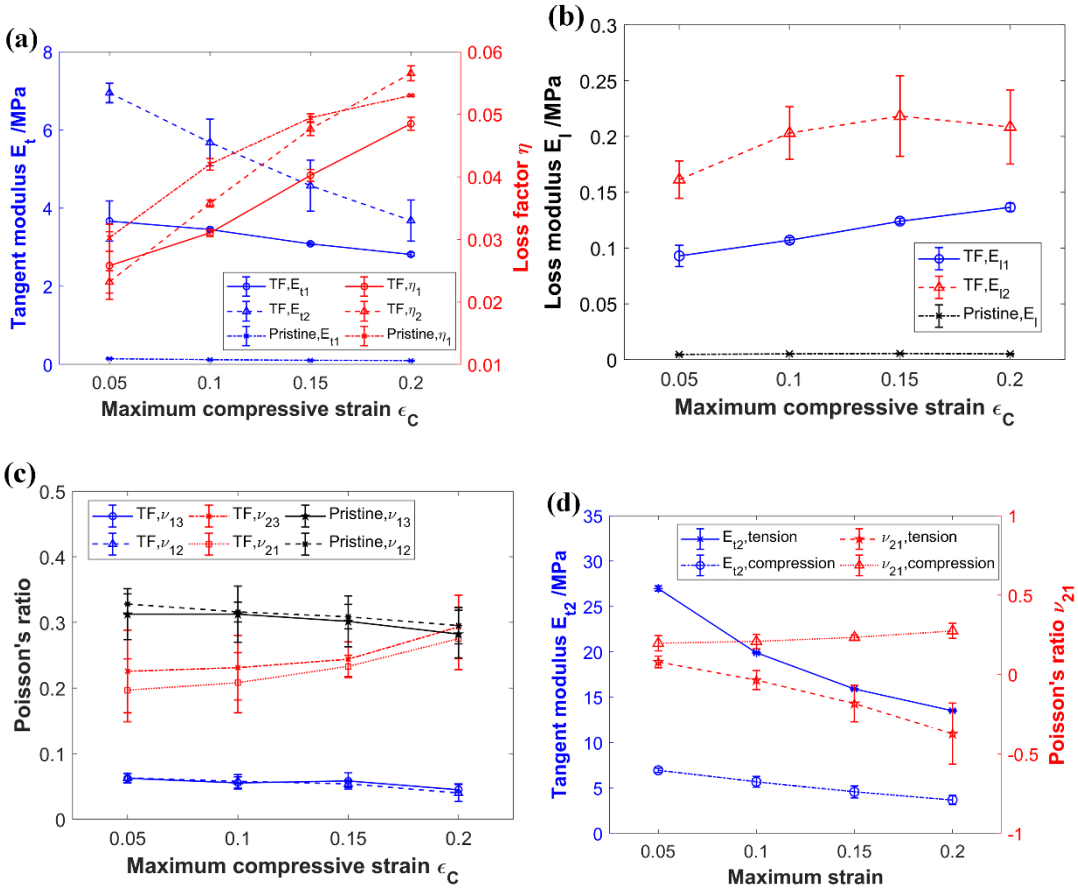

Fig. 13 Mechanical properties at 3% strain of the specimens with different maximum compressive strains. Tangent modulus and loss factor (a), loss modulus(b) and Poisson' s ratios (c). Comparison between tensile and compression tests at 3% strain when loading along direction 2 (d)

The comparison between the tensile and compression tests of the TF along direction 2 is shown in Fig. 13(d). The tensile E_{t2} modulus decreases noticeably from 27MPa to 13.5MPa as the maximum tensile strain increases from 5% to 20%. Those values are however higher than the observed reduction of the compressive E_{t2} from 6.9MPa to 3.7MPa. The tensile modulus is significantly higher than the compressive one because the elongated pore microstructures inside the TF can withstand higher loads under stretch than compression. Both the tensile and compressive moduli decrease with the maximum strain because of the reduction of the combination between convoluted ribs inside the foam and the breaking of the weak ribs caused by larger strains. The tensile Poisson' s ratio ν_{21} reduces from 0 to -0.4 with maximum tensile strain, opposite to the compressive ν_{21} case (from 0.20 to 0.28). This means the TF will always expand along the thickness direction under either transverse tension or compression. This is because the re-entrant microstructures of the TF foam in the 1-2 plane results in an auxetic behavior under tension along direction 2. The contact between ribs of the densified inner structures however lead to a lateral expansion and a positive Poisson' s ratio under compression along the direction 2. The thermoformed foams shown in this study exhibit an evident auxetic behavior, but only under transverse tensile loading.

8. Compression tests of specimens with different tensile training strains

Compression tests along the 1-direction have also been performed for the TF specimens after transverse tensile training at different strains. The training procedure of each specimen includes five loading-unloading cycles with a loading rate of 2mm/min. The results from those tests on specimens with thickness of 9mm are shown in Fig. 14. The hysteretic loops of the TF with larger tensile training strains tend to exhibit a lower slope during loading and therefore it indicates a lower stiffness. The difference is more evident in the corresponding tangent modulus curves (Fig. 14 (b)). The E_{t1} of the TF specimens with ε_T=20% increases with strain first until reaching a plateau at around 4% strain and then rise slowly again with strain. The E_{t1} increases evidently with decreasing ε_T especially within small strain ranges. When ε_T=0%, the E_{t1} curve decreases with strain first and then increases after a plateau of ~3MPa; these results agree well with those shown in Fig. 12(a). The significant reduction of E_{t1} with ε_T at small strains is mainly caused by the detachment of intertwined ribs inside the foam leading to the slight increase of specimen thickness during tensile training. The breaking of weaker ribs inside TF during training can also reduce the modulus. At large strains, the densification of inner microstructures results in the evident increase of stiffness, greatly reducing the effect of tensile train strain ε_T. The Poisson' s ratio ν_{12} varies slightly with the strain and distributes between 0 and 0.05 range, showing no noticeable effect from the value of the ε_T adopted. The results related to ν_{13} have been observed to be quite similar to the ones pertaining ν_{12} and they have not been included in this paper.

The mechanical properties at 3% strain for each specimen are shown in Fig. 14(d). The tangent modulus E_{t1} gradually reduces by 24% from 2.9MPa to 2.2MPa as the ε_T increases from 0 to 20%. The loss factor η_1 increases slightly from 0.03 to 0.04 with increasing values of ε_T. The loss modulus E_{l1} is almost constant at 0.1MPa, no matter which tensile training strain has been applied. The reduction of E_{t1} and the increase of η_1 is mainly caused by the detachment of the

intertwined ribs in the pore microstructures and again the breaking of weaker ribs inside the TF during the tensile training.

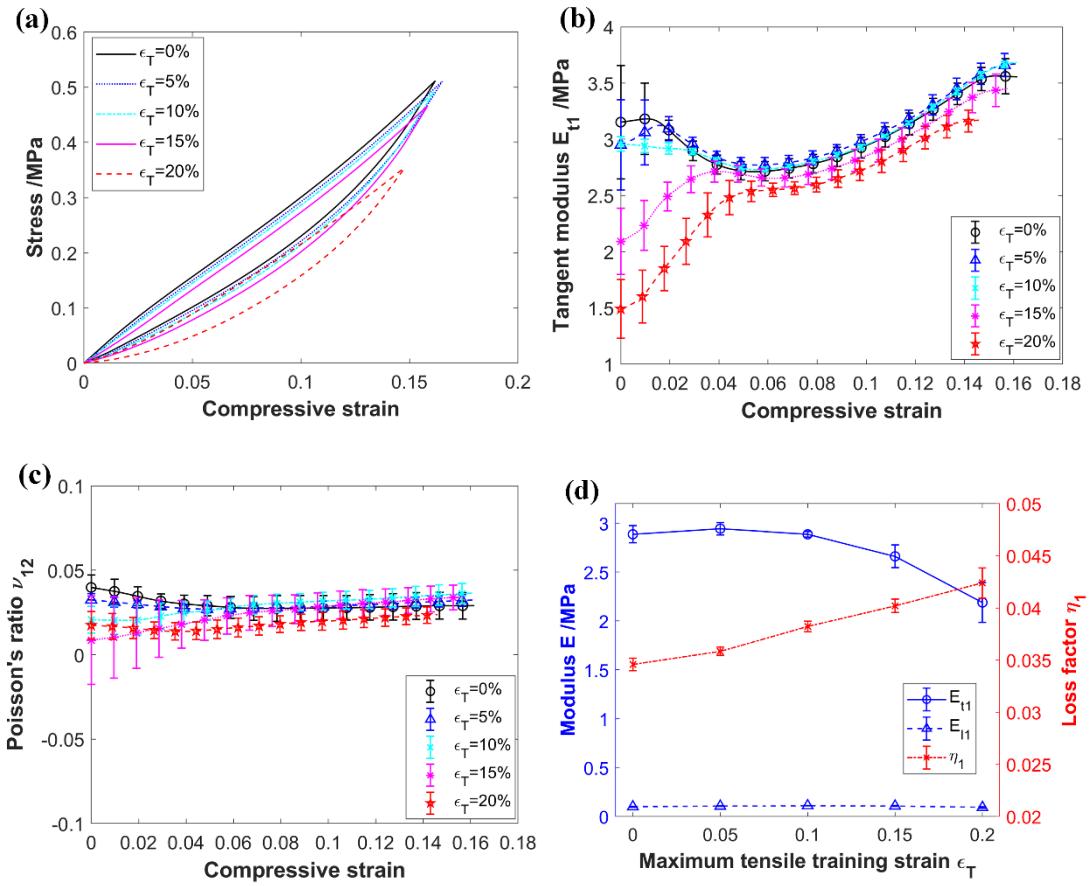

Fig. 14 Strain-dependent compressive properties of the TF specimens with 9mm thickness after tensile training. Hysteric loops (a), tangent modulus (b) and Poisson' s ratio ν_{12} (c); mechanical properties at 3% strain of specimens after tensile training of different strains (d)

The compression tests along the direction 1 of the specimens with different thickness with and without tensile training are shown in Fig. 15. The modules E_{t1} of the TF with thicknesses of 9mm and 15mm are quite similar and larger than those of the TF-5mm. This is due to the lateral shrink in the 2-3 plane of the foam block with larger thicknesses becomes more obvious during vacuuming. The densities of the TF-5mm, 9mm and 15mm are therefore 282.4kg/m^3, 315.5kg/m^3, 314.2kg/m^3 (Table 1). Although the lateral shrink of the TF-15mm during manufacturing is larger than the one present in the TF-9mm specimens, their densities are almost the same because of the higher compression ratio of the TF-9mm (from 100mm to 9mm) compared to the TF-15mm (from 150mm to 15mm). The modulus of the TF-9mm is slightly higher than the TF-15mm type, especially for specimens without tensile training. The Poisson' s ratio ν_{12} of the TF without training only increases slightly from ~0.01, ~0.04 to ~0.05 as the thickness increases from 5mm, 9mm to 15mm; this is because of the small difference in terms of inner pores microstructures caused by shrinkage in the 2-3 plane during manufacturing. The E_{t1} of the specimens with different thicknesses all show an evident reduction especially at small strains after tensile training, while the ν_{12} values slightly decrease.

As discussed above, this is mainly caused by the detachment of the convoluted ribs inside the foam leading to a slight increase of the specimen thicknesses during tensile training, and also the breaking of weaker ribs inside TF during training.

In Fig. 15 (a), the modulus of TF-9mm and TF-15mm first increases at small strains with relative large standard deviations due to the uneven and nonparallel contact surfaces between the specimen top and the compression plate of the machine (similar to the results shown in Fig. 12 (a)). If one neglects the values at small strains, the tangent modulus E_{t1} for the TF-9mm and TF-15mm first decreases due to the Mullins effect[56] and then increase with the strain due to the densification of the pores, similarly to what observed in Fig. 12 (b). The modulus of the TF-5mm increases with larger deformations and does not show reductions at small strains; this means that the densification plays a more important role in these lower density TF specimens.

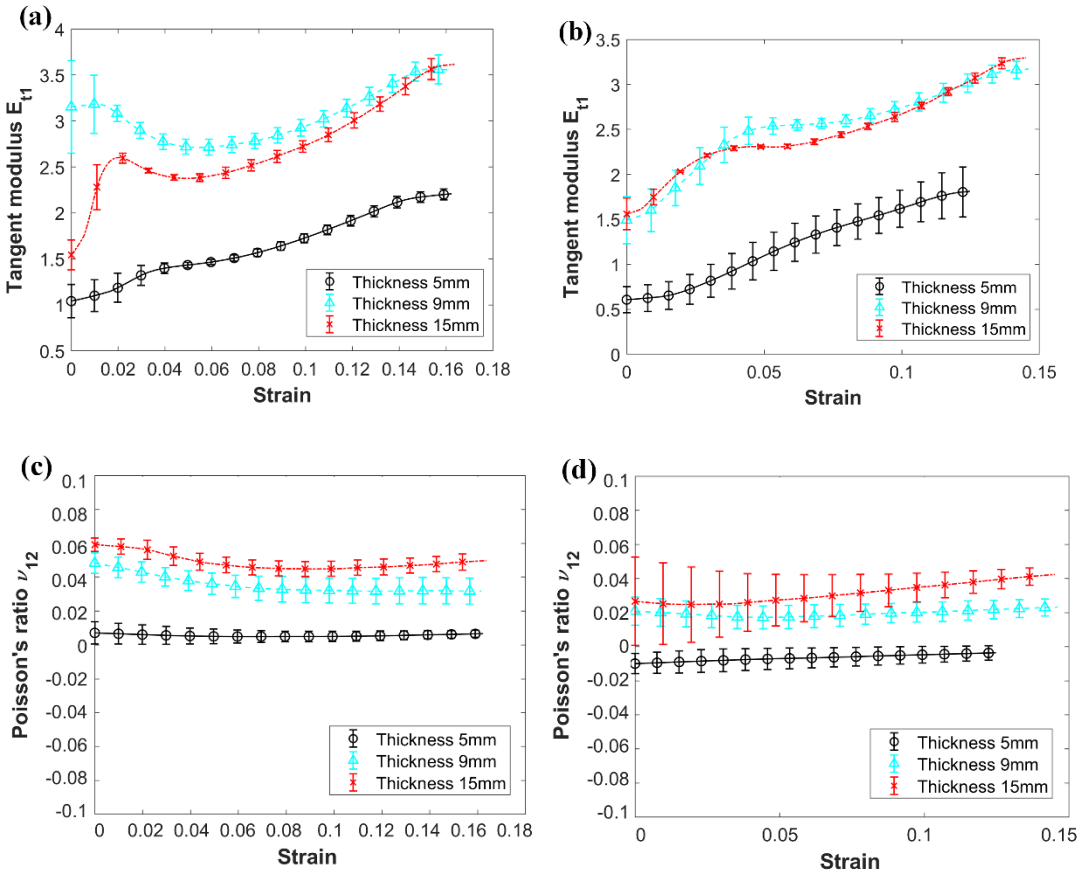

Fig. 15 Strain-dependent compressive properties of the TF specimens with different thicknesses before and after tensile training. Tangent modulus without tensile training (a); tangent modulus after tensile training of 20% strain (b); Poisson' s ratio ν_{12} without tensile training(c) and Poisson' s ratio ν_{12} after tensile training of 20% strain (d)

9. Conclusions

The tensile Young' s modulus and Poisson' s ratio of the thermoformed foam developed in this work can reach as high as 25MPa and -0.4 respectively in the 1-2 plane, with a remarkable stiffness performance compared to other auxetic foams in scientific literature, although the auxetic behavior is present in one plane only. The loss factors exhibited by these

thermoformed foams range between 2% and 6%, quite consistent with similar values identified in other auxetic foam systems. The thermoformed foam is transverse isotropic with microstructures showing elongated pores characteristics. The compressive transverse stiffness is larger than the axial one and the tensile stiffness is also significantly higher than the compressive stiffness due to the microstructural configuration of the foams. The thermoformed foam also shows some evident size effects, with thinner specimens possessing lower stiffness and larger auxeticity (up to -1.3). The tensile training can generate damage (membranes and broken cell ribs) inside the foam that results in lower stiffness and higher damping. The thermoformed foam developed in this paper can be applied in situations where high stiffness, mechanical damping and auxeticity are required. Examples of applications for which these properties are critical are – for example - vibration mat pads subjected to linear and nonlinear dynamic loading, and biomedical external supports and prosthesis. The data provided in this work are also instrumental for future designs and tests related to dynamic loading and prototyping of full or partial auxetic foams for which stiffness and energy absorption are essential characteristics.

Acknowledgement

This project has been supported by the UK Engineering and Physical Sciences Research Council (EPSRC) EP/R032793/1 SYSDYMATS. FS and HXP acknowledge the support of the University of Bristol and Zhejiang University through the InCIS-ACCIS PhD Collaboration programme and ZJU' s Overseas Academician Joint Lab for Advanced Composite Materials and Structures. HXP also acknowledges the support by the Fundamental Research Funds for the Central University.

References

1. Ren, X*., et al*., *Smart Materials and Structures* (2018) **27** (2)
2. Evans, K. E., and Alderson, A., *Advanced Materials* (2000) **12** (9), 617
3. Chan, N., and Evans, K. E., *Journal of Cellular Plastics* (1999) **35** (2), 166
4. Cheng, H. C*., et al*., *physica status solidi (b)* (2019) **256** (1)
5. Chan, N., and Evans, K. E., *Journal of Cellular Plastics* (1998) **34** (3), 231
6. Donoghue, J. P*., et al*., *physica status solidi (b)* (2009) **246** (9), 2011
7. Bezazi, A*., et al*., *physica status solidi (b)* (2009) **246** (9), 2102
8. Alderson, A*., et al*., *Composites Science and Technology* (2010) **70** (7), 1034
9. Lakes, R. S., and Witt, R., *International Journal of Mechanical Engineering Education* (2002) **30** (1), 50
10. Alderson, A*., et al*., *physica status solidi (b)* (2007) **244** (3), 817
11. Yang, S*., et al*., *Advances in Mechanical Engineering* (2015) **5**
12. Mohsenizadeh, S*., et al*., *Materials & Design* (2015) **88**, 258
13. Imbalzano, G*., et al*., *Composite Structures* (2016) **135**, 339
14. Bianchi, M., and Scarpa, F., *Smart Materials and Structures* (2013) **22** (8)
15. Bianchi, M*., et al*., *Journal of Materials Science* (2008) **43** (17), 5851
16. Allen, T*., et al*., *Procedia Engineering* (2015) **112**, 104
17. Oh, J.-H*., et al*., *Composites Part B: Engineering* (2020) **186**

18. Scarpa, F., *et al.*, *Smart Materials and Structures* (2004) **13** (1), 49
19. Howell, B., *et al.*, *Applied Acoustics* (1994) **43** (2), 141
20. Wang, Y.-C., and Lakes, R., *International Journal of Solids and Structures* (2002) **39** (18), 4825
21. Janus-Michalska, M., *et al.*, *International Journal of Applied Mechanics and Engineering* (2013) **18** (1), 55
22. Lisiecki, J., *et al.*, *physica status solidi (b)* (2013), n/a
23. Alderson, K., *et al.*, *physica status solidi (b)* (2012) **249** (7), 1322
24. Critchley, R., *et al.*, *physica status solidi (b)* (2013), 20
25. Lakes, R. S., *Science* (1987) **235**, 1038
26. Chan, N., and Evans, K. E., *Journal of Materials Science* (1997) **32** (22), 5945
27. Duncan, O., *et al.*, *Acta Materialia* (2017) **126**, 426
28. Mohsenizadeh, S., *et al.*, *physica status solidi (b)* (2019) **256** (10)
29. Scarpa, F., *et al.*, *physica status solidi (b)* (2005) **242** (3), 681
30. Pierron, F., *The Journal of Strain Analysis for Engineering Design* (2010) **45** (4), 233
31. McDonald, S. A., *et al.*, *physica status solidi (b)* (2011) **248** (1), 45
32. Boba, K., *et al.*, *ACS Appl Mater Interfaces* (2016) **8** (31), 20319
33. Chan, N., and Evans, K. E., *Journal of Materials Science* (1997) **32** (21), 5725
34. Li, Y., and Zeng, C., *Adv Mater* (2016) **28** (14), 2822
35. Grima, J. N., *et al.*, *Advanced Engineering Materials* (2009) **11** (7), 533
36. Bianchi, M., *et al.*, *Acta Materialia* (2011) **59** (2), 686
37. Wang, Y.-C., *et al.*, *Cellular Polymers* (2001) **20** (6), 373
38. Bianchi, M., *et al.*, *Acta Materialia* (2010) **58** (3), 858
39. Duncan, O., *et al.*, *physica status solidi (b)* (2019) **256** (1)
40. Cadamagnani, F., *et al.*, *physica status solidi (b)* (2009) **246** (9), 2118
41. Duncan, O., *et al.*, *Smart Materials and Structures* (2016) **25** (5)
42. Imbalzano, G., *et al.*, *Composite Structures* (2018) **183**, 242
43. Allen, T., *et al.*, *physica status solidi (b)* (2015) **252** (7), 1631
44. Mohanraj, H., *et al.*, *physica status solidi (b)* (2016) **253** (7), 1378
45. Chan, N., and Evans, K. E., *Journal of Cellular Plastics* (1999) **35** (2), 130
46. Rueger, Z., *et al.*, *physica status solidi (b)* (2019) **256** (1)
47. Li, D., *et al.*, *physica status solidi (b)* (2017) **254** (12)
48. Rueger, Z., and Lakes, R. S., *Smart Materials and Structures* (2016) **25** (5)
49. Bianchi, M., *et al.*, *Journal of Materials Science* (2010) **45** (2), 341
50. Lisiecki, J., *et al.*, *physica status solidi (b)* (2014) **251** (2), 314
51. Beatty, M. F., and Stalnaker, D. O., *Journal of Applied Mechanics* (1986) **53** (4), 807
52. Ogden, R. W., and Roxburgh, D. G., *Proceedings of the Royal Society of London. Series A: Mathematical, Physical and Engineering Sciences* (1999) **455** (1988), 2861
53. Zhang, D., *et al.*, *Materials Science and Engineering: A* (2013) **580**, 305
54. Monica Carfagni, E. L., Marco Pierini, *Proceedings-spie the international society for optical engineering* (1998) **1**, 580
55. Orban, F., *Journal of Physics: Conference Series* (2011) **268**
56. Prisacariu, C., *Polyurethane Elastomers: From Morphology to Mechanical Aspects*. Springer Vienna: 2011
57. Karasudhi, P., *Foundations of Solid Mechanics*. Springer Netherlands: 1991

58. Zhu, H. X.*, et al.*, *Journal of the Mechanics and Physics of Solids* (1997) **45** (11-12), 1875
59. Dement'ev, A. G.*, et al.*, *Polymer Mechanics* (1975) **9** (1), 37
60. Rinde, J. A., *Journal of Applied Polymer Science* (1970) **14** (8), 1913